Acta Biochim Biophys Sin 2025, 57(x): 1–14
https://cstr.cn/32197.14.abbs.2025056
https://doi.org/10.3724/abbs.2025056
Original Article

Original Article

Triptonide facilitates autophagy-mediated apoptosis in esophageal squamous cell carcinoma by targeting the AMPK-mTOR-ULK1 axis

Jiujun Ju[1,2,†], Nuo Xu[1,2,†], Bohan Li[1,2], Dan Shi[1,2], Jiahui Cai[1,2], Qiusheng Zheng[1,2], Lei Ye[1,2,*], Shaosen Zhang[3,*], and Caixia Wang[1,2,*]

[1]Featured Laboratory for Biosynthesis and Target Discovery of Active Components of Traditional Chinese Medicine, School of Traditional Chinese Medicine, Binzhou Medical University, Yantai 264003, China, [2]Collaborative Innovation Platform for Modernization and Industrialization of Regional Characteristic Traditional Chinese Medicine, School of Traditional Chinese Medicine, Binzhou Medical University, Yantai 264003, China, and [3]Department of Etiology and Carcinogenesis, National Cancer Center/Cancer Hospital, Chinese Academy of Medical Sciences and Peking Union Medical College, Beijing 100021, China

[†]These authors contributed equally to this work.

*Correspondence address. Tel: +86-535-6916303; E-mail: cxwang@bzmc.edu.cn (C.W.) / E-mail: zhangss@cicams.ac.cn (S.Z) / E-mail: bzmcyelei@163.com (L.Y.)

Received 21 June 2024 Accepted 17 December 2024 Published 20 June 2025

Abstract

Triptonide (TN) is a small-molecule compound initially derived from *Tripterygium wilfordii* Hook. f used in traditional Chinese medicine. However, its potential antitumor mechanisms are still far from adequately understood. The purpose of this research is to elucidate the antitumor and pharmacological effects of TN on esophageal squamous cell carcinoma (ESCC). Functional assays, such as CCK-8 and colony formation assays, are used to evaluate the effects of TN on KYSE450 and KYSE510 cells. Subsequently, western blot analysis, Hoechst 33258 staining, flow cytometric analysis, autophagic flux detection, and transmission electron microscopy (TEM) are used to determine the effects of TN on apoptosis and autophagy in ESCC cells. Additionally, the autophagy inhibitor 3-methyladenine (3-MA) and the AMPK inhibitor dorsomorphin (Compound C, CC) are administered to explore the molecular mechanisms and crucial pathways in ESCC cells. Our findings provide strong evidence that TN induces autophagy-dependent apoptosis by targeting the AMPK-mTOR-ULK1 axis in ESCC cells. Collectively, this study sheds light on the anticancer mechanisms of TN in esophageal squamous cell carcinoma and suggests that TN is a promising candidate for the antitumor phytomedicine.

Key words triptonide, esophageal squamous cell carcinoma, AMPK-mTOR-ULK1, apoptosis, autophagy

Introduction

Esophageal cancer has gradually become a serious international health issue, and its potential health impact is currently a highly topical focus of concern [1]. Esophageal cancer mainly consists of two histopathological subtypes, squamous cell carcinoma (SCC) and adenocarcinoma (AC) [2], of which SCC accounts for 90% of all cases of esophageal cancer globally and is highly prevalent in Asia, East Africa, and South America; however, AC is more common in developed countries and is the most common form of esophageal cancer in the US [3]. Esophageal cancer has the sixth highest overall global mortality rate and the seventh highest global incidence [4–6]. Therefore, owing to its high degree of malignancy, esophageal cancer should be prevented as early as possible. However, esophagectomy is a severe surgical treatment with potential dangers and complications [7]. Therefore, there is an urgent need to discover more dependable, efficient, and secure anticancer medications that can be utilized as alternatives or in addition to surgery to enhance treatment outcomes[8].

Natural products offer exceptional prospects for the discovery of innovative agents/active templates, particularly in the field of anticancer medication [9,10]. Chinese herbal medicines, the primary sources of natural products, are becoming increasingly popular owing to their remarkable therapeutic ability in biological systems. Therefore, we performed a comprehensive analysis to

investigate the antitumor effects of these herbs on tumor cells. We investigated the antitumor effects and mechanisms of triptonide (TN), an ingredient obtained from the Chinese herb *Tripterygium wilfordii* Hook. f (TwHF). TwHF is extensively used to treat various dermatological and rheumatological disorders [11,12]. Owing to its combination therapy and new dosage form, the potential pharmacological activity of TwHF is currently a highly topical focus of concern [13]. TN not only possesses superior pharmacological properties, such as anti-inflammatory activity [14,15], antiandrogenic fertility [16] and antitumor properties [17], but is also less toxic than triptolide. Triptolide, which is also the main active ingredient in TwHF, is known as one of the most likely natural medicinal compounds to be developed into a modern drug [18,19]. TN has no noticeable toxic side effects at 20 times the effective dose *in vivo* [20]. However, studies on the inhibitory effect of TN on esophageal squamous cell carcinoma (ESCC) are lacking.

Autophagy, a type II programmed cell death pathway, is essential in cancer and contributes to all aspects of tumor formation, including tumor creation, growth, progression, and continuous survival [21–23]. Autophagy activation causes apoptosis, resulting in autophagy-mediated cell death [24]. Autophagy-mediated cell death must rigorously adhere to the criterion that the inhibition of autophagy reduces cell death, whether genetically or pharmacologically [25]. Autophagy pathways are supported by various ATG proteins and their main components, such as UNC-51-like kinase-1 (ULK1) and LC3 [26–28]. ULK1 was found to be an immediate target of mammalian target of rapamycin (mTOR) and adenosine 5′-monophosphate (AMP)-activating protein kinase (AMPK), indicating its important role as a cancer cell nutrition sensor/integrator that controls the autophagy process [29]. Therefore, an in-depth study of the interaction between tumor autophagy and apoptosis is essential for the development of effective anticancer drugs.

In the present study, we examined the functional and anticancer therapeutic potential of TN in ESCC cells. We discovered that TN inhibited ESCC cell growth in a dose-dependent manner and further investigated whether TN influences apoptosis by inducing autophagy in ESCC cells. We also explored the specific signaling pathways involved in this process to better understand the precise mechanism of its anticancer activity. We hope that this research will open avenues for future studies on the application of traditional Chinese medicine. These findings provide valuable insights into the application of TN in the treatment of ESCC, which may contribute to improving treatment choices for patients with this type of cancer.

Materials and Methods

Cell culture

ESCC cell lines derived from human mainly include KYSE450 (#1430) and KYSE510 (#1436) were obtained from Japanese Collection of Research Bioresources (Osaka, Japan) and maintained in RPMI 1640 medium (Sigma-Aldrich, St Louis, USA) supplemented with 10% fetal bovine serum (FBS; ExCell Bio, Suzhou, China) and no more than 1% antibiotic solution (Solarbio, Beijing, China) at 37 °C in a humidified environment of 5% CO_2 [30].

Reagents and associated antibodies

The TN (HY-32736-99607), 3-MA (HY-19312-149211), and CC (HY-13418A) strains used in this study were purchased from MedChem Express (Monmouth Junction, USA). The primary antibodies used consisted of caspase-3 (66470-2-Ig, 1:1000), caspase-9 (66169-1-Ig, 1:1000), cleaved caspase-9 (66169-1-Ig, 1:1000), BAD (67830-1-Ig, 1:2000), phospho-p70 (S6K) (Thr389) (28735-1-AP, 1:1500), mTOR (66888-1-Ig, 1:20,000), p-mTOR (Ser2448) (67778-1-Ig, 1:10,000), ULK1 (20986-1-AP, 1:3000), and LC3 (14600-1-AP, 1:1000) from Proteintech (Chicago, USA), cleaved caspase-3 (9664s, 1:800), AMPK (2532S, 1:2000), p-AMPK (2535S, 1:800), and p-ULK1 (Ser757) (14202s, 1:800) from Cell Signaling Technology (Beverly, USA), p62 (PM045, 1:2000) from MBL (Beijing, China), and β-actin (TA-09, 1:1000) from ZSGB-BIO (Beijing, China), and Ki67 (GB111499, 1:1000) from Servicebio (Wuhan, China).

Cell viability assay

The viability of KYSE450 and KYSE510 cell lines was measured via a detection kit (CCK8; Biosharp, Hefei, China) according to the manufacturer's instructions. Briefly, cells were cultured in 96-well plates and grown in 100 μL of RPMI 1640 medium (containing 10% FBS). After 12 h, cells attached to the wells and were subsequently treated with TN at increasing concentrations (0, 40, 80, and 160 nM) over periods of 24, 48, or 72 h, respectively. After incubation, CCK-8 was added into each well and incubated at 37°C for approximately 2 h before the absorbance at 450 nm was measured with a micro-ELISA reader (Tecan, Männedorf, Switzerland).

Colony formation assay

ESCC cells were evenly seeded into 12-well plates at a density of 1000 cells per well and cultivated for one week. After one week, the cells were treated with various concentrations of TN (0, 40, 80 and 160 nM) for 24 h. The prepared cells were cultured in RPMI 1640 medium for two to three weeks until colonies appeared [31]. The cells were subsequently gently washed with phosphate buffer solution (PBS, pH 7.3–7.5), treated with 4% tissue fixing solution (BL539A; Biosharp) for 16 min, and stained with 0.1% crystal violet staining solution (BL802A; Biosharp) for 7 min. Finally, the colonies were observed and counted under a DMI3000B inverted fluorescence microscope (Leica, Wetzlar, Germany) and images were captured with a camera.

Hoechst 33258 staining

The ESCC cells were treated with different concentrations (0, 40, 80, and 160 nM) of TN for 24 h. Then, the cells were fixed with the 4% tissue fixing solution and stained with Hoechst 33258 solution (Solarbio) in the dark for 10 min. After the process of staining, the cells were washed with PBS three times. Finally, images were captured via the DMI3000B inverted fluorescence microscope.

Apoptosis analysis via flow cytometry

Apoptosis of ESCC cells was measured via an apoptosis detection kit (TransGen Biotech, Beijing, China). Briefly, ESCC cells (2×10^5 cells/well) were seeded into six-well plates and incubated with different concentrations of TN (0, 40, 80 or 160 nM) for 24 h. These cells were digested with Trypsin-EDTA Free (Solarbio) for approximately 4 min at 37°C, and then collected, washed three times with PBS, and stained for 10 min in complete darkness with Annexin V-FITC/PI reagent (100 μL 1× binding buffer, 5 μL Annexin V-FITC, 5 μL PI). Finally, cell apoptosis was examined with a flow cytometer (BD FACSCalibur, Franklin Lakes, USA).

Autophagic flux detection

The mCherry-GFP-LC3B plasmid (Beyotime Biotechnology, Shanghai, China) was introduced into ESCC cells via Lipofectamine 3000

(Thermo Fisher Scientific, Waltham, USA). The medium was changed after 7 h, and the cells were treated with TN, 3-MA, or CC for 24 h. Then, at room temperature, the cells were placed in the 4% fixative solution for 20 min. Subsequently, the coverslips were removed from the fixative solution and mounted on glass slides using an antifade mounting medium (Solarbio). Fluorescence microscopy was employed to follow and image the cells in glass slides via a Stellaris 5 laser scanning confocal microscope (Leica) at 40× magnification.

Transmission electron microscopy (TEM) images of autophagosomes

After 24 h of TN treatment or no treatment, the ESCC cells were trypsinized with Trypsin-EDTA (Solarbio) and subsequently fixed in 2.5% glutaraldehyde (Biosharp) at 4°C. The material was then dehydrated after being fixed in a 1% osmium tetroxide solution (Sinopharm Chemical Reagent, Shanghai, China). After embedding, the collected samples were sliced into 50 nm slices. Finally, the samples were photographed via an HT7800 transmission electron microscope (Hitachi, Tokyo, Japan).

Western blot analysis

RIPA lysis buffer (Solarbio), PMSF (Solarbio), and phosphatase inhibitor (Solarbio) are mixed at a ratio of 1 mL:10 μL:10 μL to prepare the protein lysis buffer. Samples are lysed for 30 min, and the supernatant is collected for protein quantification using a BCA assay kit (Solarbio). Proteins were denatured at 100°C, and equal amounts were separated by 8%–12% SDS-PAGE electrophoresis [32]. The separated proteins were subsequently transferred to polyvinylidene fluoride membranes (Merck Millipore, Billerica, USA), blocked for 4 h at room temperature with 5% fat-free dried milk, and incubated with the respective antibodies for 12 h at 4°C. Subsequently, the anti-mouse IgG or anti-rabbit IgG was added and incubated for 40 min at 37°C. The membranes were then subjected visualization using an enhanced chemiluminescence (ECL) assay kit (Biosharp). Finally, the densities of the blots were determined and quantified via ImageJ software (10.8.1v; NIH, Bethesda, USA).

Tumor xenograft experiments

Nude mice (Jinan Pengyue Experimental Animal Breeding Co., Ltd., Jinan, China), weighing about 16–17 g and aged 6–8 weeks, were utilized in experiments following Binzhou Medical University's animal ethics guidelines and housed in an experimental animal room that meets the specific pathogen-free (SPF) standard. KYSE450 cells were suspended in PBS, mixed with Matrigel and subcutaneously (5×10^6 cells/200 μL) injected into the armpits of the mice. When the size of the tumors reached approximately 10 mm, the mice were randomly divided into control and TN therapy groups. Every other day, the TN group was intraperitoneally injected with TN solution at a dose of 10 mg/kg, while the control group was intraperitoneally injected with an equal volume of saline. During the experiment, the nude mice were weighed every other day, and the tumors were measured using vernier calipers. Tumor volume was calculated via the formula: $V = (\text{length} \times \text{width}^2)/2$. At the end of the experiment, the mice were euthanized, and the tumors and major organs were collected for subsequent examination and analyses.

Histological analysis

Tissues including the heart, liver, spleen, and kidneys were fixed with 4% paraformaldehyde (Biosharp) for more than 24 h. Subsequently, after dehydration, the tissues were embedded in wax blocks and sectioned at a thickness of 4 μM, which were then deparaffinized, treated with graded ethanol, and finally rinsed with distilled water. For further examination, the sections were stained with hematoxylin solution (Servicebio) for 3–5 min, and then stained with eosin solution (Servicebio) for another 5 min, finally mounted with neutral gum (Sinopharm Chemical Reagent).

For immunohistochemistry (IHC) analysis, tumor samples were also subjected to paraffin embedding and sectioning, followed by deparaffinization and rehydration. The samples were then incubated in peroxidase blocking solution (Beyotime Biotechnology) for 25 min and blocked with 3% BSA (Servicebio). The samples were then incubated with Ki67 primary antibody at 4°C for 16 h before being exposed to an HRP-conjugated anti-rabbit IgG secondary antibody (Servicebio) at room temperature for 50 min. Finally, the samples were stained with 3,3′-diaminobenzidine tetrahydrochloride (DAB; G1212-200T; Servicebio) and counterstained with hematoxylin (Servicebio), observed, and photographed under the DMI3000B inverted fluorescence microscope.

Liver and kidney function analysis

The detection of liver and kidney function indicators (ALT, AST, CREA, and BUN) was completed with a fully automatic Chemray 240 biochemical analyser from Rayto(Shenzhen, China). Firstly, blood was collected into a 1.5-mL centrifuge tube by means of orbital blood collection and was allowed to stand at room temperature for 30 min. Subsequently, the blood sample was centrifuged at 16,100 *g* for 15 min to separate the upper serum. Then, the upper serum was quickly frozen and stored in an environment of –80 °C. Finally, the serum was processed using the alanine aminotransferase assay kit (Rayto), aspartate aminotransferase assay kit (Rayto), Urea Assay Kit (Rayto), and Creatinine Assay Kit (Rayto), and then analyzed on an automatic biochemical analyzer (Rayto) for testing.

Statistical analysis

Data were presented as the mean ± standard error (SEM) from at least three separate experiments. The quantitative assessment was performed using GraphPad Prism 8. Student's *t* test was used to analyze the significant differences between two groups. When comparing three or more groups, one-way analysis of variance (ANOVA) was employed to explore whether there were significant differences among these groups. Statistical significance was set at $P < 0.05$.

Results

TN inhibits the viability of ESCC cells *in vitro*

TN is a natural product candidate (Figure 1A) and has beneficial pharmacological traits, including antiandrogenic properties. However, the anti-cancer effect and underlying mechanisms of TN on ESCC remains poorly understood. The inhibitory effects of TN on ESCC cell proliferation were dose- and time-dependent, and the IC_{50} values for KYSE450 and KYSE510 cells were 91.03 nM and 118.3 nM, respectively (Figure 1B,C), after 48 h drug treatment. Through light microscopic morphology observation, we found that the number of cells decreased as the TN concentration increased, and the cell morphology became rounder and less adhesive (Figure 1D). The results of colony formation experiments demonstrated that TN

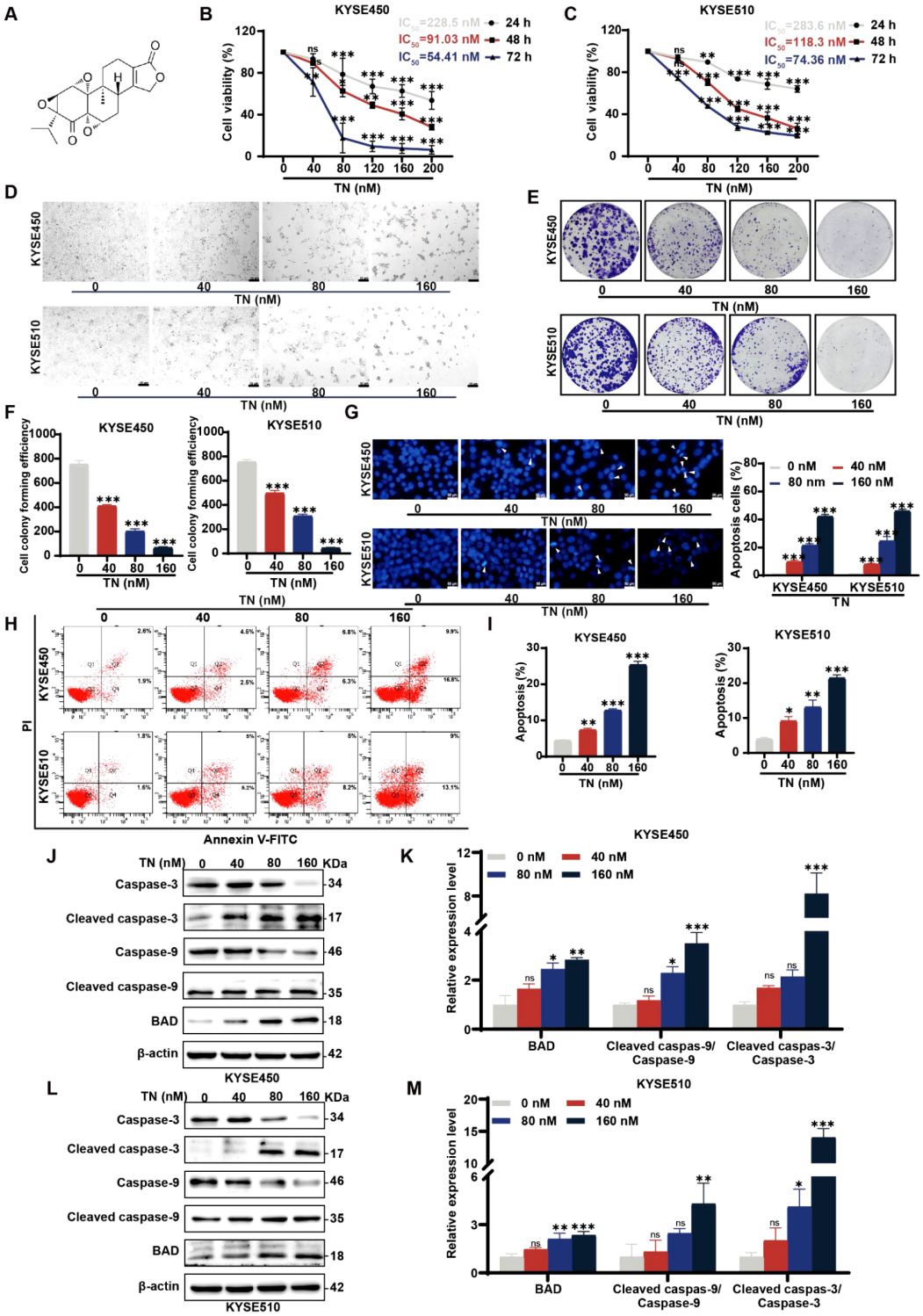

Figure 1. TN inhibits the proliferation of ESCC cells and induces apoptosis (A) The chemical structure of TN. (B,C) KYSE450 and KYSE510 cells were exposed to TN at increasing doses for up to 72 h to detect the influence of TN on ESCC cell proliferation and calculate the IC_{50} values of ESCC cells at 24, 48 and 72 h. (D) Bright-field images of KYSE450 and KYSE510 cells that were treated with TN for 24 h at concentrations of 0, 40, 80, and 160 nM. Scale bar: 10 μm. (E,F) The ability of KYSE450 and KYSE510 cells to form colonies after being exposed to TN at increasing concentrations (0, 40, 80, and 160 nM) for 24 h. (G) Pictures of KYSE450 and KYSE510 cells stained with Hoechst 33258. Scale bar: 50 μm. The quantitative results revealed that the TN-treated ESCC cells were apoptotic. (H,I) ESCC cells were treated with increasing concentrations of TN (0, 40, 80, or 160 nM) for 24 h, and apoptosis was determined by flow cytometry. (J–M) Western blot analysis was conducted to evaluate the expression levels of BAD, cleaved caspase-3, caspase-3, cleaved caspase-9, and caspase-9 in KYSE450 and KYSE510 cells after treatment with increasing concentrations (0, 40, 80, and 160 nM) of TN for 24 h. Data are presented as the mean ± SEM ($n = 3$). $^{*}P < 0.05$, $^{**}P < 0.01$, $^{***}P < 0.001$.

dramatically decreased the number of colonies (Figure 1E,F). According to the aforementioned results, TN inhibits the viability and proliferation of ESCC cells.

TN promotes apoptosis in ESCC cells

To assess the effect of TN on apoptosis in ESCC cells, we stained the cells with Hoechst 33258. The results revealed that after TN treatment, ESCC cells exhibited much stronger nuclear fluorescence staining, implying cell apoptosis (Figure 1G). Results from flow cytometry analysis further demonstrated that ESCC cell apoptosis was promoted after exposure to different concentrations (40, 80, and 160 nM) of TN for 24 h (Figure 1H,I). Additionally, flow cytometry confirmed the upregulation of critical apoptosis regulators, with significant increases in BAD protein levels and activation of both caspase-9 and caspase-3, as evidenced by elevated cleaved forms (Figure 1J–M). These results illustrate that TN induces the apoptosis of ESCC cells.

TN induces autophagy in ESCC cells

Autophagy and apoptosis are closely controlled processes that underlie cellular and tissue homeostasis, progression and disease. To explore whether TN can induce autophagy in ESCC cells and its progression, we utilized fluorescence colocalization analysis with the mCherry-GFP-LC3B plasmid to assess autophagic flux [33]. In the process of autophagy, the mCherry-GFP-LC3B fusion protein localizes to the autophagic membrane. The merging of red and green fluorescence results in yellow spots, indicating the formation of autophagosomes (GFP^+RFP^+). In autolysosomes with an acidic pH, GFP is quenched and appears as red spots [34–36]. We observed a significant increase in the number of yellow (GFP^+RFP^+) spots in ESCC cells treated with TN compared with the control cells (Figure 2A,B), indicating enhanced autophagosome formation. TEM revealed the presence of double-membraned vesicles in ESCC cells after treatment with TN (80 nM) compared with control cells (Figure 2C), and these vesicles were verified as signs of increased autophagy. In addition, western blot analysis results revealed that p62 (SQSTM1) expression was downregulated at elevated TN concentrations (40, 80, and 160 nM), whereas LC3-II/LC3-I levels were substantially elevated (Figure 2D,E). These findings indicate that TN substantially induced autophagy in ESCC cells in a dose-dependent manner.

Autophagy inhibition decreases TN-induced apoptosis in ESCC cells

To explore the mechanism by which TN induces the participation of ESCC cells in autophagy and apoptosis, we investigated the relationship between autophagy and apoptosis in the presence of 3-MA, an early-stage autophagy inhibitor. It was demonstrated that 3-MA reduced the ratio of yellow puncta (GFP^+RFP^+) (Figure 3A,B). Similarly, according to the western blot analysis data, the combination of TN and 3-MA significantly diminished LC3-II/LC3-I expression and enhanced p62 (SQSTM1) expression during autophagic flux in ESCC cells (Figure 3C,D). Furthermore, according to the flow cytometry results, compared with treatment with TN alone, cotreatment with 3-MA and TN substantially decreased the cell apoptosis rate (Figure 4A–D). In the TN-treated group, 3-MA

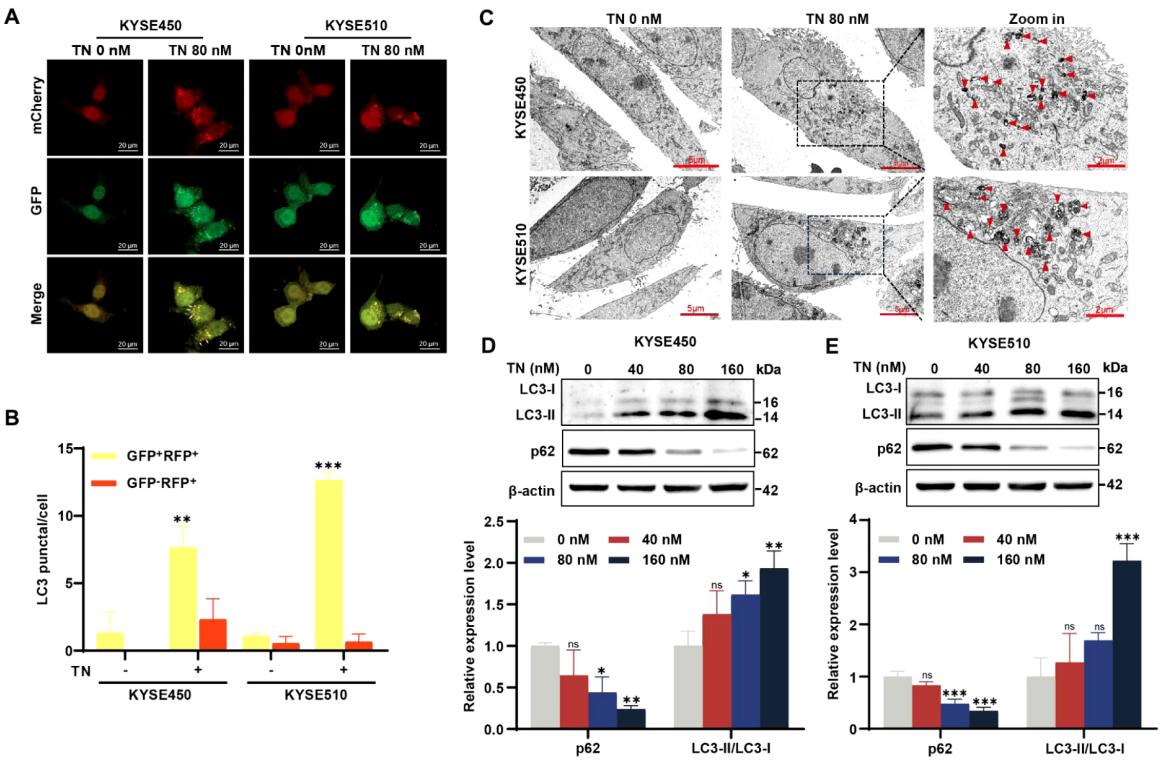

Figure 2. TN induces autophagy in ESCC cells (A) Representative images of KYSE450 and KYSE510 cells, either treated or not treated with TN (80 nM) for 24 h and then transfected with mCherry-GFP-LC3B. Scale bar: 20 μm. (B) Analysis of the number of red (GFP^-RFP^+) and yellow (GFP^+RFP^+) puncta in all groups. (C) Transmission electron microscopy images of KYSE450 and KYSE510 cells, either treated or not treated with TN (80 nM) for 24 h. Scale bar: 2 or 5 μm. (D,E) The levels of p62, LC3 I, and LC3 II in KYSE450 and KYSE510 cells were assessed via western blot analysis after treatment with or without TN (80 nM) for 24 h. Data are presented as the mean ± SEM ($n = 3$). $^*P < 0.05$, $^{**}P < 0.01$, $^{***}P < 0.001$.

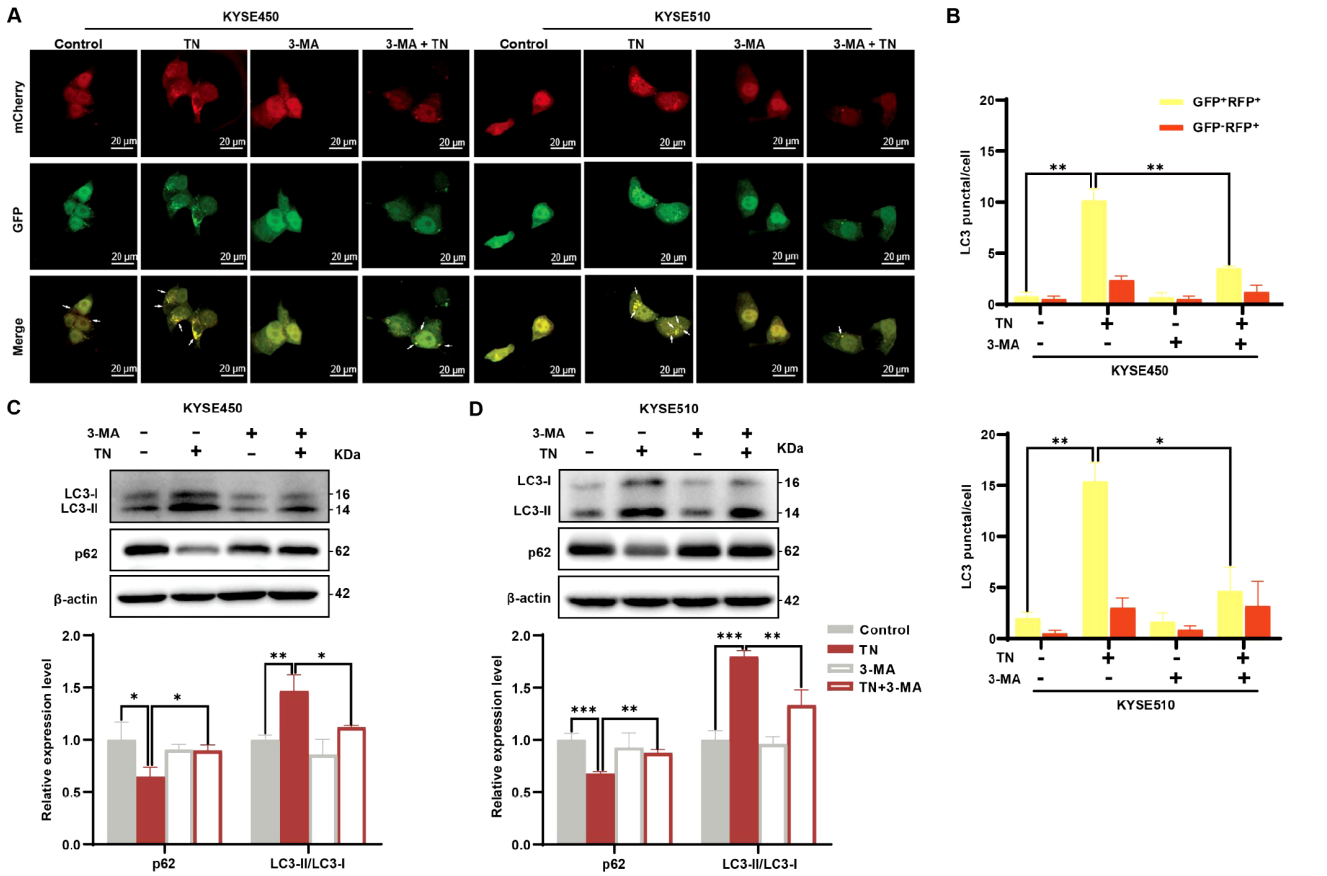

Figure 3. 3-MA inhibits TN-induced autophagy (A) Typical images of KYSE450 and KYSE510 cells treated or not treated with TN (80 nM) or 3-MA (2 mM) for 24 h and transiently transfected with mCherry-GFP-LC3B. Scale bar: 20 μm. (B) Analysis of the number of red ($GFP^{-}RFP^{+}$) and yellow ($GFP^{+}RFP^{+}$) puncta in all groups. (C,D) The levels of p62, LC3 I, and LC3 II in KYSE450 and KYSE510 cells were assessed via western blot analysis after treatment with or without TN (80 nM) in the presence or absence of 3-MA (2 mM) for 24 h. Data are presented as the mean ± SEM ($n = 3$). $^{*}P < 0.05$, $^{**}P < 0.01$, $^{***}P < 0.001$.

drastically decreased the levels of the apoptosis-associated proteins cleaved caspase-3/caspase-3, cleaved caspase-9/caspase-9 and BAD (Figure 4E,F). These data demonstrate that TN induces apoptosis by promoting autophagy in ESCC cells.

TN-induced autophagy in ESCC cells is controlled via the AMPK-mTOR-ULK1 signaling pathway

AMPK is involved in autophagy and influences the manner in which cells respond to energy stress. Under the stress of dietary sufficiency, increasing mTOR activity can suppress ULK1 activation by phosphorylating ULK1 at Ser757 and breaking the connection between ULK1 and AMPK. To further examine the mechanisms involved in TN-induced apoptosis in ESCC cells by promoting autophagy, the expression of AMPK-mTOR-ULK1 signaling pathway proteins was examined in the TN-treated group. We found that the activation of p-AMPK (Thr172) diminished p-mTOR (Ser2448), p-ULK1 (Ser757), and phospho-p70 (S6K) (Thr389) in a dose-dependent manner (Figure 5A,B). The combination of 3-MA and TN contributed to a reduction in p-AMPK (Thr172) and an increase in p-mTOR (Ser2448), p-ULK1 (Ser757), and phospho-p70 (S6K) (Thr389) during the process of TN treatment (Figure 5C,D).

Additionally, to verify the involvement of this pathway, we tested the effect of the AMPK inhibitor CC [37–39]. When ESCC cells were treated with TN and CC simultaneously, we observed a decrease in the protein expression levels of phospho-p70 (S6K), p-AMPK, p-mTOR, and p-ULK1 (Figure 6A,B). Confocal fluorescence microscopy revealed that the combination treatment of TN and CC led to a restoration in the proportion of yellow puncta ($GFP^{+}RFP^{+}$) (Figure 7A,B). We subsequently examined the expression levels of the autophagy markers LC3 and p62 in the presence of CC. However, compared with incubation with TN alone, coincubation with TN and CC resulted in an increased expression level of the p62 protein and a decreased LC3-II/LC3-I ratio (Figure 7C,D). These findings indicate that CC inhibits TN-induced autophagy in KYSE450 and KYSE510 cells, indicating that the AMPK-mTOR-ULK1 signaling axis plays a crucial role in TN-induced autophagy.

TN-induced autophagy mediates apoptosis via the AMPK-mTOR-ULK1 axis in ESCC cells

Stimulation of the AMPK-mTOR-ULK1 axis can induce autophagy-mediated apoptosis in various human cancers. To elucidate the role of this pathway, we utilized the AMPK inhibitor CC to regulate its activity. Flow cytometry analysis revealed that CC significantly reduced the apoptotic rate of ESCC cells induced by TN (Figure 8A–D). According to the western blot analysis, CC drastically diminished the expression levels of apoptotic proteins, such as cleaved caspase-3/caspase-3, cleaved caspase-9/caspase-9, and

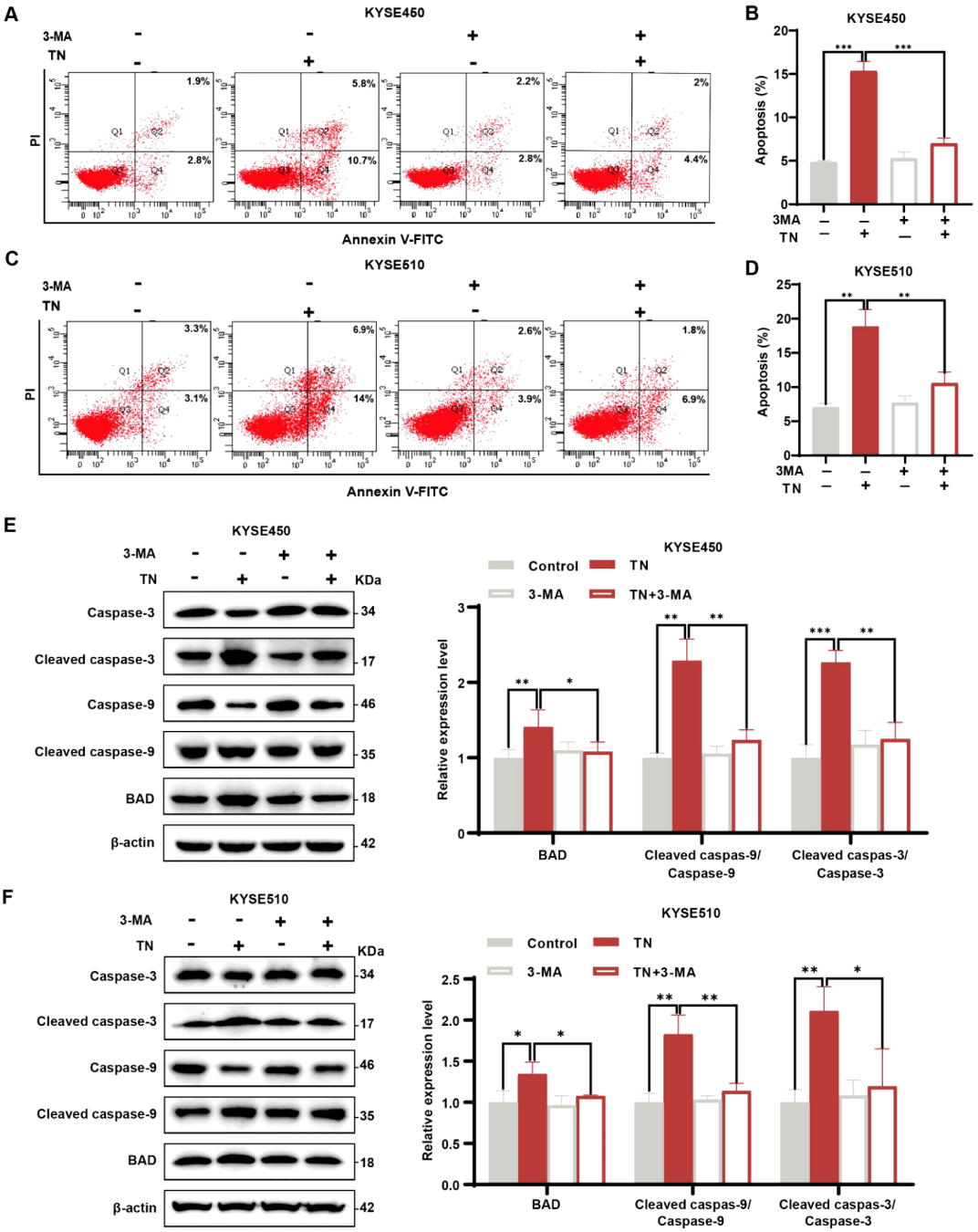

Figure 4. Autophagy inhibition decreases TN-induced apoptosis (A–D) Flow cytometry was used to assess the degree of apoptosis in KYSE450 and KYSE510 cells exposed to TN (80 nM) with or without 3-MA for 24 h. (E,F) Apoptosis-associated protein expression levels were examined through a western blot analysis in KYSE450 and KYSE510 cells treated with TN (80 nM) in the presence or absence of 3-MA (2 mM) for 24 h. Data are presented as the mean ± SEM ($n = 3$). $^{*}P < 0.05$, $^{**}P < 0.01$, $^{***}P < 0.001$.

BAD (Figure 8E,F). These results further verified that TN induces autophagy-mediated apoptosis via the AMPK-mTOR-ULK1 axis in ESCC cells.

TN inhibits the growth of ESCC tumor xenografts *in vivo*

To investigate the antitumor effects of TN *in vivo*, we established an ESCC xenograft model by subcutaneously injecting KYSE450 cells into nude mice. On the basis of the size of the ESCC tumors, these nude mice were randomly assigned to either the control group or the TN treatment group. During the 3-week study period, the TN treatment group received intraperitoneal injections of 10 mg/kg TN every other day, whereas the control group was administered an equivalent volume of saline. Compared with those in the control group, the xenograft tumors in the TN treatment group presented significant reductions in both tumor weight and volume, with no significant effect on the overall body weight of the mice during treatment (Figure 9A–D). IHC quantitative analysis revealed that TN treatment dramatically decreased the proportion of Ki-67-

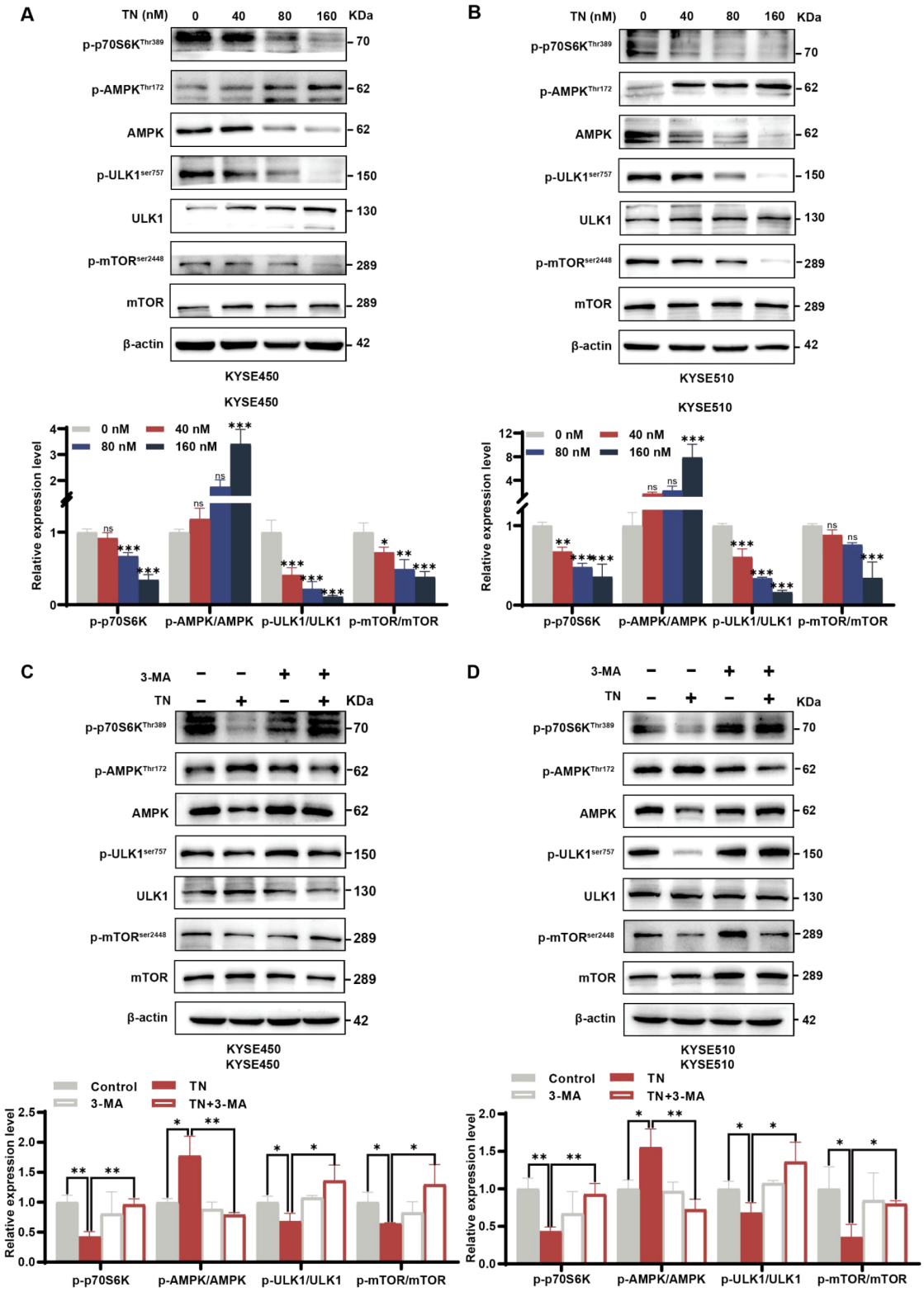

Figure 5. The autophagy inhibitor 3-MA suppresses the TN-stimulated AMPK-mTOR-ULK1 axis (A,B) Western blot analysis was performed to examine the expression levels of p-AMPK (Thr172), AMPK, p-ULK1 (Ser757), ULK1, p-mTOR (Ser2448), mTOR and phospho-p70 (S6K) (Thr389) in KYSE450 and KYSE510 cells exposed to various concentrations (0, 40, 80, or 160 nM) of TN for 24 h. (C,D) Western blot analysis was performed to examine the expression levels of p-AMPK (Thr172), AMPK, p-ULK1 (Ser757), ULK1 and phospho-p70 (S6K) (Thr389) in KYSE450 and KYSE510 cells after 24 h of treatment with or without TN (80 nm), in the presence or absence of 3-MA (2 mM). Data are presented as the mean ± SEM ($n = 3$). $^{*}P < 0.05$, $^{**}P < 0.01$, $^{***}P < 0.001$.

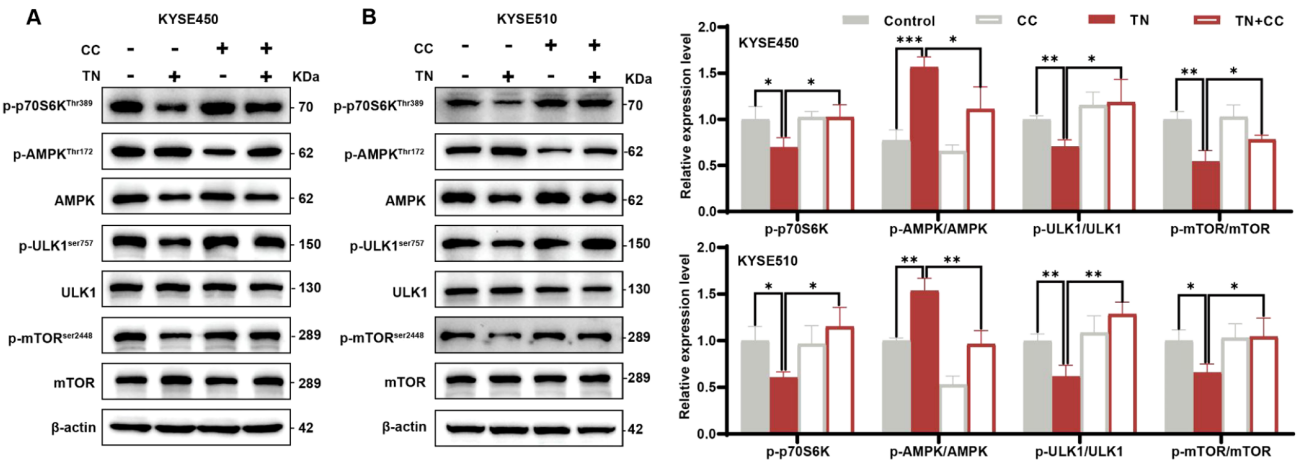

Figure 6. The inhibitor CC prevents the TN-mediated activation of the AMPK-mTOR-ULK1 axis (A,B) Western blot analysis was carried out to examine the levels of p-AMPK (Thr172), AMPK, p-ULK1 (Ser757), ULK1, p-mTOR (Ser2448), mTOR and phospho-p70 (S6K) (Thr389) in KYSE450 and KYSE510 cells cultured with or without TN (80 nM) in the presence or absence of CC (10 μM) for 24 h. Data are presented as the mean ± SEM ($n = 3$). $^{*}P < 0.05$, $^{**}P < 0.01$, $^{***}P < 0.001$.

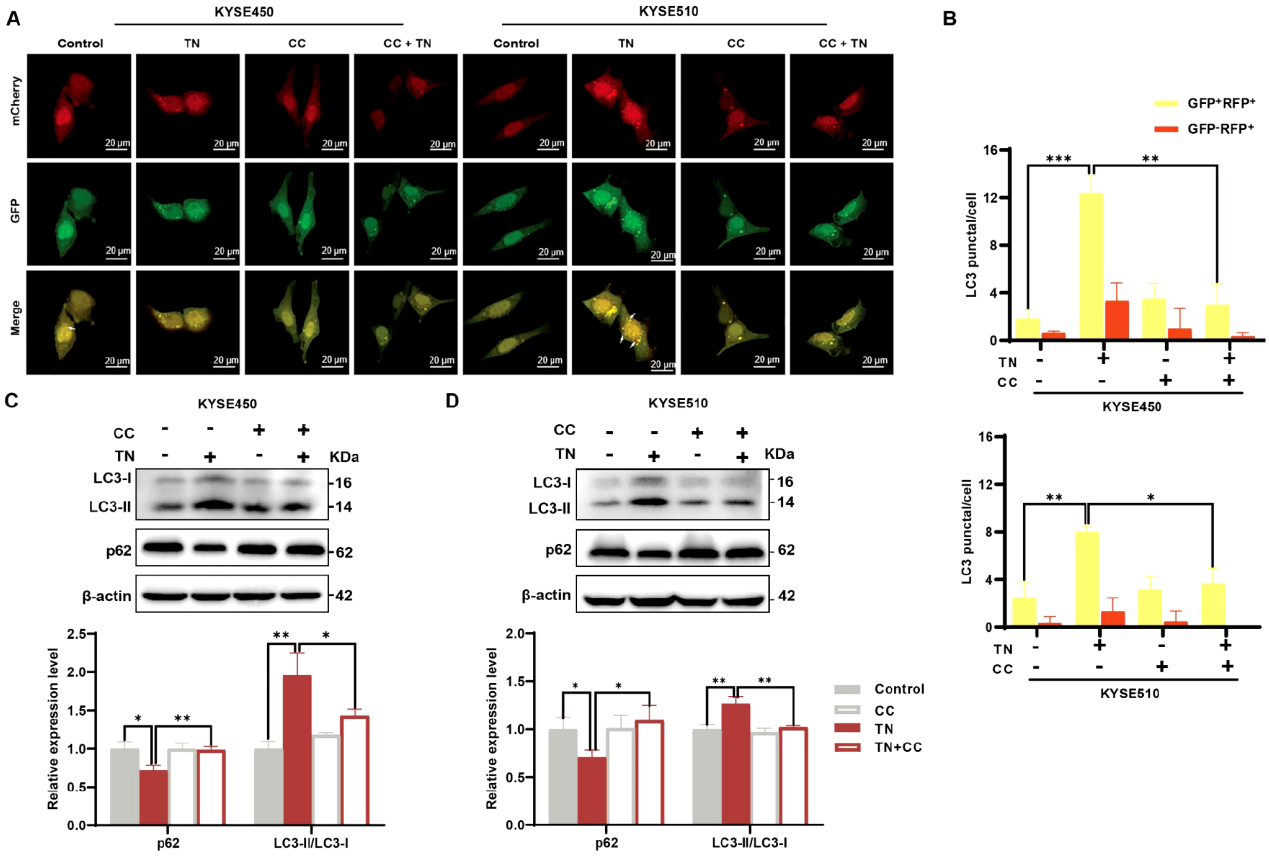

Figure 7. The AMPK inhibitor CC prevents TN-induced autophagy (A,B) Typical images of KYSE450 and KYSE510 cells that were either treated or not treated with TN (80 nM) in the presence or absence of CC (10 μM) for 24 h and then transfected with mCherry-GFP-LC3B. Scale bar: 20 μm. Qualitative analysis revealed that red ($GFP^{-}RFP+$) and yellow ($GFP^{+}RFP^{+}$) puncta were present in all the groups. (C,D) The expression levels of p62, LC3 II and LC3 I was determined via western blot analysis in KYSE450 and KYSE510 cells treated with or without TN (80 nM) and in the presence or absence of CC (10 μM) for 24 h. Data are presented as the mean ± SEM ($n = 3$). $^{*}P < 0.05$, $^{**}P < 0.01$, $^{***}P < 0.001$.

positive cells in tumor tissues (Figure 9E,F), demonstrating that TN inhibits ESCC cell proliferation. Western blot analysis results revealed changes in apoptosis and autophagy markers in ESCC tissues treated with TN: increased expression levels of cleaved caspase-3/caspase-3, cleaved caspase-9/caspase-9, BAD, LC3-II/LC3-I, and p-AMPK (Thr172) but decreased expression levels of phospho-p70 (S6K) (Thr389), p-mTOR (Ser2448), p-ULK1 (Ser757), and p62 were observed (Figure 9G,H). These outcomes are

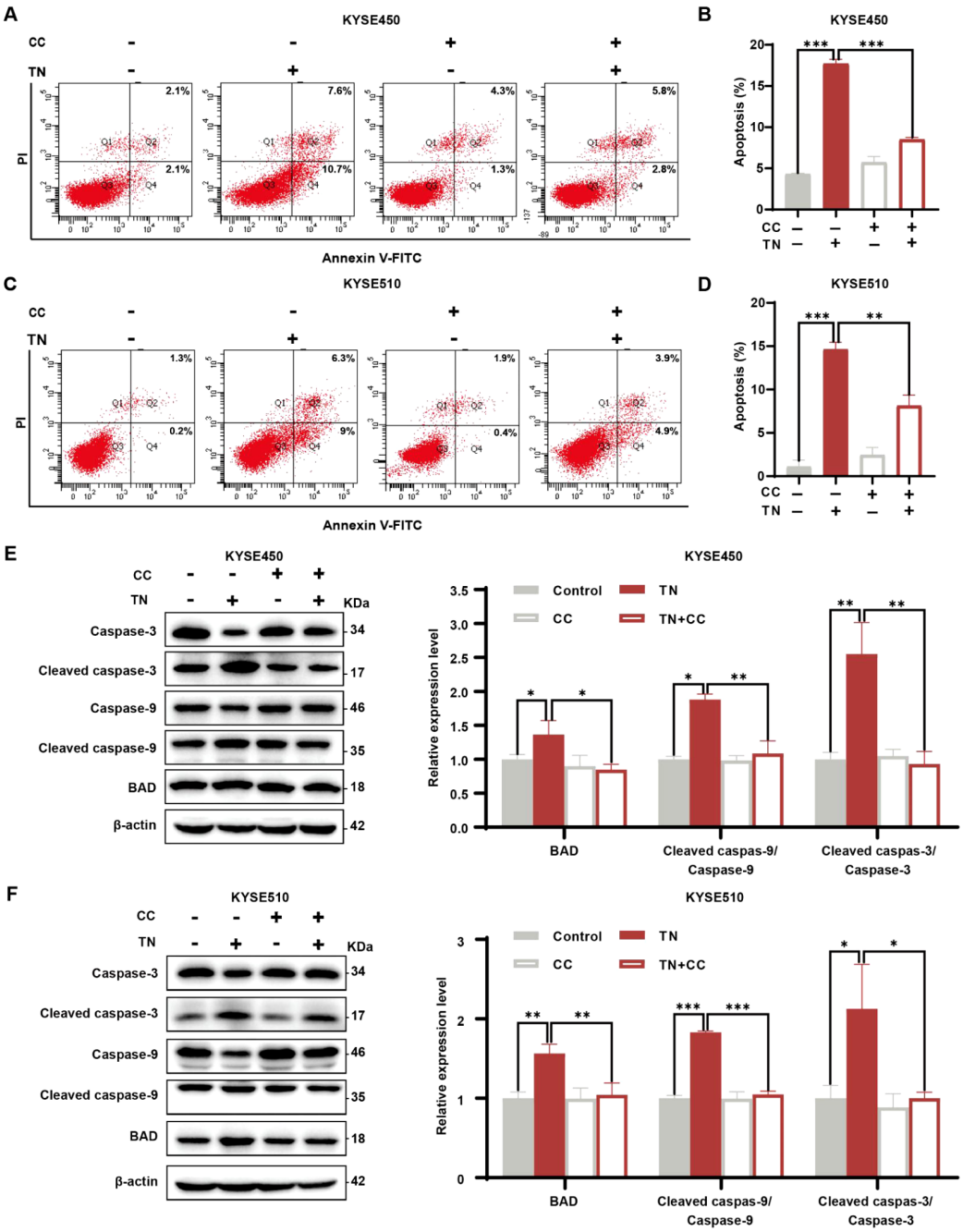

Figure 8. The influence of the AMPK inhibitor CC on TN-induced apoptosis (A–D) The apoptosis rates of KYSE450 and KYSE510 cells were examined after treatment with or without TN (80 nM) and in the presence or absence of CC (10 μM) for 24 h. (E,F) The expression levels of BAD, cleaved caspase-3, caspase-3, cleaved caspase-9, and caspase-9 were measured via western blot analysis in KYSE450 and KYSE510 cells treated with or without TN (80 nM) and in the presence or absence of CC (10 μM) for 24 h. Data are presented as the mean ± SEM ($n = 3$). $^{*}P < 0.05$, $^{**}P < 0.01$, $^{***}P < 0.001$.

consistent with the trends observed *in vitro*, further confirming the crucial role of TN in inducing autophagy-dependent apoptosis in ESCC cells. To further assess the toxicological profile of TN in mice, we performed H&E staining analysis on critical organ tissues including the liver, heart, spleen and kidneys. It was observed that there were no notable differences in organ structure between the control group and the TN-treated group (Figure 9I). Furthermore, serological analysis revealed that there were no statistically significant differences in the concentrations of key biochemical markers such as ALT, AST, CREA, and BUN between the TN-treated group and the control group (Figure 9J–M), confirming the low toxicity of TN. Overall, these findings suggest that TN effectively suppresses the growth of ESCC tumors *in vivo* while exhibiting excellent biosafety.

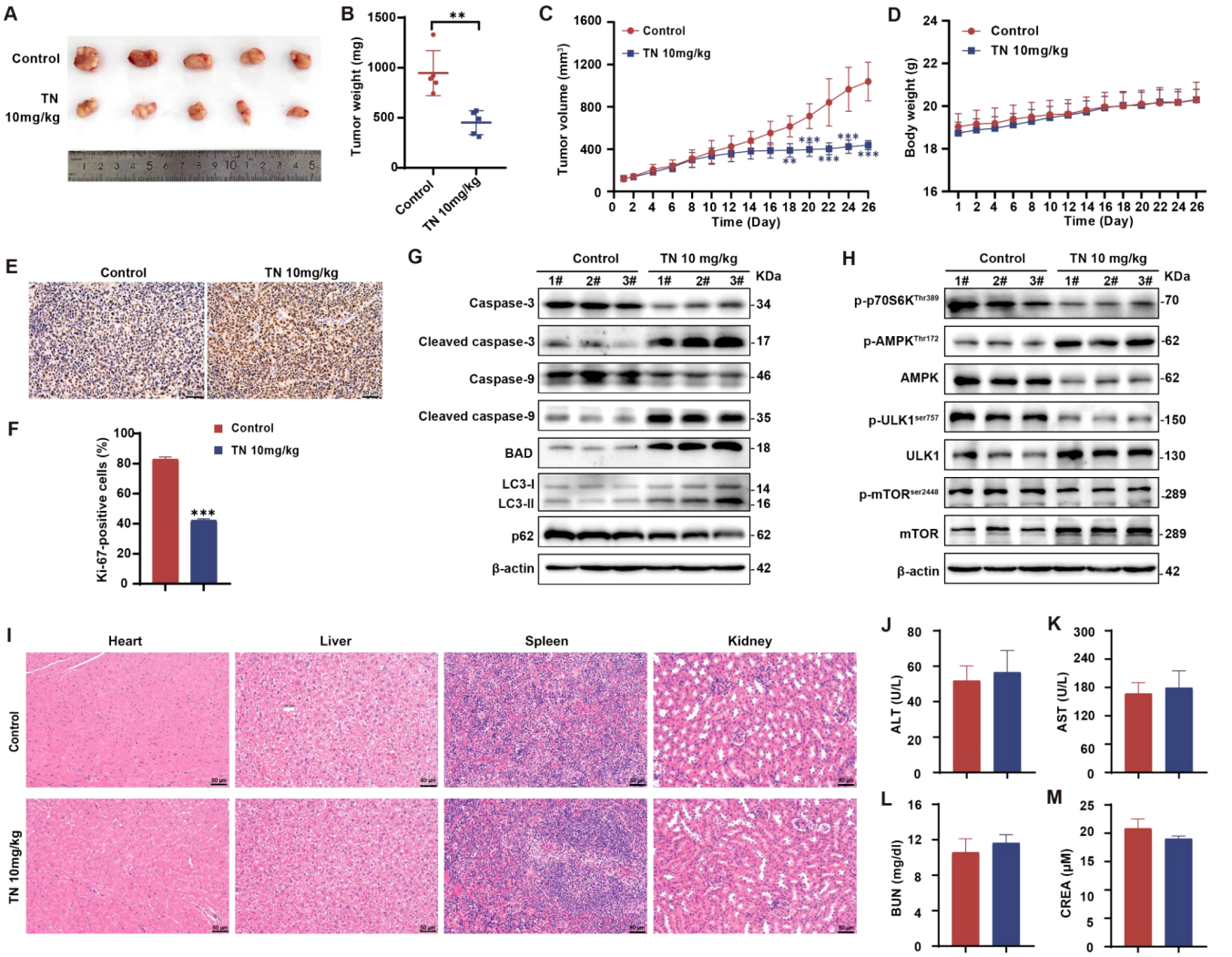

Figure 9. TN inhibits the growth of ESCC tumor xenografts in nude mice (A) Images of ESCC tumors excised from the control group and the TN (10 mg/kg) group of nude mice. (B) Weights of the removed tumor xenografts from each group. (C) Growth curve illustrating the variations in tumor volume in each group over an increasing number of days. (D) Growth curve showing the changes in body weight of the mice in each group over a series of days. (E,F) IHC images of Ki-67 and quantitative analysis of Ki-67-positive cells in each group of tumor tissues. Scale bar: 50 μm. (G,H) Bad, cleaved caspase-3, cleaved caspase-9/caspase-9, p62, LC3 II, LC3 I, p-ULK1 (Ser757), ULK1, p-mTOR (Ser2448), mTOR, p-AMPK (Thr172), AMPK, and phospho-p70 (S6K) (Thr389) expression levels in tumor tissues in the control and TN (10 mg/kg) groups was detected via western blot analysis. (I) H&E staining images of heart, liver, spleen, and kidney tissues collected from each group of mice. Scale bar: 50 μm. (J–M) Serum ALT, AST, BUN, and CREA levels in each group. Data are presented as the mean ± SEM ($n = 5$). *$P < 0.05$, **$P < 0.01$, ***$P < 0.001$.

Discussion

Natural products are valuable resources of compounds for drug development. Owing to their excellent therapeutic properties and biological compatibility, natural products such as traditional Chinese medicines are gaining increasing attention in the discovery of anticancer chemicals. TN is a small molecule initially isolated from the traditional Chinese medicine plant TwHF. These results indicated that TN has anticancer properties in ESCC cells, and further investigations revealed that apoptosis and autophagy occur concurrently. Notably, TN-induced autophagy enhanced apoptosis via the AMPK-mTOR-ULK1 axis.

A substantial percentage of esophageal cancers are unresectable at diagnosis, and the majority of patients who are cured eventually relapse, making esophageal cancer a formidable and deadly disease worldwide [40]. Therefore, identifying innovative biological pathways and improving treatment approaches to increase the survival rates of patients with esophageal cancer are essential. Autophagy plays a dual role in tumor development, both in protecting against and inhibiting cell growth. Understanding the role of autophagy and apoptosis in esophageal cancer is vital for revealing its pathology and identifying new treatment strategies. Studies have shown that TN can inhibit ovarian cancer cell proliferation by inducing apoptosis and autophagy [41], suggesting potential mechanisms in esophageal cancer. However, the specific effects of TN on esophageal cancer need further research. Numerous studies have shown critical roles for cancer stem cells (CSCs) and Myc expression in ESCC [42,43]. Notably, the efficacy of TN in suppressing CSCs, Myc expression, and the growth of breast cancer cells has been reported [44]. Inspired by

these findings, we aimed to explore the potential mechanisms underlying the action of TN in the treatment of ESCC.

Apoptosis, autophagy, and necrosis are the three primary morphologically distinct types of cell death in multicellular organisms. All three types can be carried out via different, and sometimes overlapping, signaling pathways activated in response to certain stimuli [7]. Therefore, these interactions are crucial for enhancing cancer treatment and patient outcomes [45,46]. Numerous stress mechanisms gradually induce autophagy and apoptosis inside the same cell, regulating the cellular and organismal turnover of organelles and proteins, respectively. In conclusion, autophagy prevents the development of apoptosis, whereas the activation of caspases related to apoptosis prevents autophagy. Nevertheless, under certain circumstances, autophagy or autophagy-related proteins could be beneficial for inducing apoptosis, resulting in "autophagic cell death" [47]. Autophagy is critical for the cytotoxic effects of numerous chemotherapeutic medications, and the pharmacological suppression of autophagy with 3-methylidene (3-MA) diminishes the cytotoxicity of these treatments [48].

Furthermore, prior studies have investigated the antitumor effect of TN in breast cancer cells, prostate cancer cells, colon cancer cells, and nasopharyngeal carcinoma cells [44,49–51], but the intricate interplay between apoptosis and autophagy in TN-induced ESCC cells has yet to be established. In the present study, we found that TN increased the levels of LC3-II/LC3-I and decreased the level of p62, a marker protein of autophagy, indicating that TN could induce autophagy. To further elucidate how TN affects autophagy, experiments were conducted to detect variations in autophagy-related proteins and determine autophagy flux via the autophagy inhibitor 3-MA induced by TN. The results demonstrated that inhibiting autophagy with 3-MA substantially decreased sensitivity to TN therapy and ESCC apoptosis. Autophagy-mediated apoptosis was observed in TN-treated ESCC cells.

The expression of mTOR on the lysosomal surface is blocked in nutrient-deficient environments, whereas autophagy is promoted by ULK1 dephosphorylation [52]. The AMPK and mTORC1 pathways serve as crucial regulators that integrate cellular nutrient and energy signals to maintain cellular homeostasis by modulating anabolic and catabolic processes, including autophagy [53]. ULK1 is an essential inducer of autophagosome formation. By phosphorylating the downstream targets involved in autophagy, ULK1 promotes the synthesis of protein complexes essential for the autophagosome [54]. mTORC1 strictly regulates autophagy by inhibiting autophagy induction through phosphorylation-dependent regulation of ULK1/2 and the VPS34 complex [55,56]. AMPK is an essential regulator of cellular energy metabolism that activates ULK1 at Ser317 and Ser777 by indirectly inactivating mTOR, leading to the dephosphorylation of ULK1 at Ser757 [57–59]. mTORC1 can decrease ULK1 activity by phosphorylating ULK1 at Ser 757 and damaging its interaction with AMPK [60,61].

The AMPK-mTOR-ULK1 pathway can activate many types of cancer cells, suggesting that it may be a latent breakthrough for cancer therapy [30,62]. Our results revealed that TN significantly increased AMPK phosphorylation at Thr172, decreased ULK1 phosphorylation at Ser757, and decreased mTOR phosphorylation at Ser2448. When ESCC cells were treated alone or in combination with TN, *AMPK* silencing resulted in decreased autophagy and reduced apoptosis. These findings reveal that the AMPK-mTOR-ULK1 axis plays an indispensable role in autophagy-mediated apoptosis.

Collectively, these results revealed that TN is a potential natural anticancer substance for treating ESCC. TN induces autophagy-mediated apoptosis via the AMPK-mTOR-ULK1 signaling pathway. The bioactivity of TN against cancer and its underlying mechanisms were demonstrated for the first time. However, the clinical application of TN is frequently prescribed for the whole plant. The current study only clarified the primary chemical components. In the future, we will investigate the composition of TwHF and identify its active components. These findings provide a novel understanding of the molecular mechanisms underlying the potential anti-ESCC effects of TN, suggesting that TN is a promising therapeutic option for ESCC.

Funding

This work was supported by the grants from the National Key R&D Program of China (No. 2023YFC3503200 and 2023YFC3503205) and the Scientific Research Foundation of Binzhou Medical University (No. BY2020KYQD15).

Conflict of Interest

The authors declare that they have no conflict of interest.

References

1. Siegel RL, Miller KD, Wagle NS, Jemal A. Cancer statistics, 2023. *CA Cancer J Clin* 2023, 73: 17–48
2. Morgan E, Soerjomataram I, Rumgay H, Coleman HG, Thrift AP, Vignat J, Laversanne M, ***et al.*** The global landscape of esophageal squamous cell carcinoma and esophageal adenocarcinoma incidence and mortality in 2020 and projections to 2040: new estimates from GLOBOCAN 2020. *Gastroenterology* 2022, 163: 649–658.e2
3. Enzinger PC, Mayer RJ. Esophageal cancer. *N Engl J Med* 2003, 349: 2241–2252
4. Urba S. Esophageal cancer: preoperative or definitive chemoradiation. *Ann Oncol* 2004, 15: iv93–iv96
5. Puhr HC, Prager GW, Ilhan-Mutlu A. How we treat esophageal squamous cell carcinoma. *ESMO Open* 2023, 8: 100789
6. Sung H, Ferlay J, Siegel RL, Laversanne M, Soerjomataram I, Jemal A, Bray F. Global cancer statistics 2020: GLOBOCAN estimates of incidence and mortality worldwide for 36 cancers in 185 countries. *CA Cancer J Clin* 2021, 71: 209–249
7. Lagergren J, Lagergren P. Recent developments in esophageal adenocarcinoma. *CA Cancer J Clin* 2013, 63: 232–248
8. Huang K, Zhang B, Feng Y, Ma H. Magnolol promotes the autophagy of esophageal carcinoma cells by upregulating *HACE1* gene expression. *Acta Biochim Biophys Sin* 2024, 56: 1044–1054
9. Newman DJ, Cragg GM. Natural products as sources of new drugs over the nearly four decades from 01/1981 to 09/2019. *J Nat Prod* 2020, 83: 770–803
10. Xiang X, Tian Y, Hu J, Xiong R, Bautista M, Deng L, Yue Q, ***et al.*** Fangchinoline exerts anticancer effects on colorectal cancer by inducing autophagy via regulation AMPK/mTOR/ULK1 pathway. *Biochem Pharmacol* 2021, 186: 114475
11. Zhang Y, Mao X, Li W, Chen W, Wang X, Ma Z, Lin N. *Tripterygium wilfordii*: an inspiring resource for rheumatoid arthritis treatment. *Med Res Rev* 2021, 41: 1337–1374
12. Wu C, Jin HZ, Shu D, Li F, He CX, Qiao J, Yu XL, ***et al.*** Efficacy and Safety of *Tripterygium wilfordii* Hook F versus acitretin in moderate to severe psoriasis vulgaris. *Chin Med J* 2015, 128: 443–449
13. Song J, He GN, Dai L. A comprehensive review on celastrol, triptolide and triptonide: insights on their pharmacological activity, toxicity, combina-

tion therapy, new dosage form and novel drug delivery routes. *Biomed Pharmacother* 2023, 162: 114705
14. Zhang T, Rao Q, Dai M, Wu ZE, Zhao Q, Li F. *Tripterygium wilfordii* protects against an animal model of autoimmune hepatitis. *J EthnoPharmacol* 2023, 309: 116365
15. Luo Y, Hou X, Xi A, Luo M, Wang K, Xu Z. Tripterygium wilfordii Hook F combination therapy with methotrexate for rheumatoid arthritis: an updated meta-analysis. *J EthnoPharmacol* 2023, 307: 116211
16. Chang Z, Qin W, Zheng H, Schegg K, Han L, Liu X, Wang Y, ***et al.*** Triptonide is a reversible non-hormonal male contraceptive agent in mice and non-human primates. *Nat Commun* 2021, 12: 1253
17. Jin D, Yu M, Li X, Wang X. Efficacy of *Tripterygium wilfordii* Hook F on animal model of diabetic kidney diseases: a systematic review and meta-analysis. *J EthnoPharmacol* 2021, 281: 114536
18. Noel P, Von Hoff DD, Saluja AK, Velagapudi M, Borazanci E, Han H. Triptolide and its derivatives as cancer therapies. *Trends Pharmacol Sci* 2019, 40: 327–341
19. Tong L, Zhao Q, Datan E, Lin GQ, Minn I, Pomper MG, Yu B, ***et al.*** Triptolide: reflections on two decades of research and prospects for the future. *Nat Prod Rep* 2021, 38: 843–860
20. Lin M, Hua R, Ma J, Zhou Y, Li P, Xu X, Yu Z, ***et al.*** Bisphenol A promotes autophagy in ovarian granulosa cells by inducing AMPK/mTOR/ULK1 signalling pathway. *Environ Int* 2021, 147: 106298
21. Baehrecke EH. Autophagy: dual roles in life and death? *Nat Rev Mol Cell Biol* 2005, 6: 505–510
22. Degenhardt K, Mathew R, Beaudoin B, Bray K, Anderson D, Chen G, Mukherjee C, ***et al.*** Autophagy promotes tumor cell survival and restricts necrosis, inflammation, and tumorigenesis. *Cancer Cell* 2006, 10: 51–64
23. Miller DR, Thorburn A. Autophagy and organelle homeostasis in cancer. *Dev Cell* 2021, 56: 906–918
24. Patra S, Praharaj PP, Klionsky DJ, Bhutia SK. Vorinostat in autophagic cell death: a critical insight into autophagy-mediated, -associated and -dependent cell death for cancer prevention. *Drug Discov Today* 2022, 27: 269–279
25. Denton D, Kumar S. Autophagy-dependent cell death. *Cell Death Differ* 2019, 26: 605–616
26. Liu P, Xu Y, Ye J, Tan J, Hou J, Wang Y, Li J, ***et al.*** Qingre Huazhuo Jiangsuan Decoction promotes autophagy by inhibiting PI3K/AKT/mTOR signaling pathway to relieve acute gouty arthritis. *J EthnoPharmacol* 2023, 302: 115875
27. Debnath J, Gammoh N, Ryan KM. Autophagy and autophagy-related pathways in cancer. *Nat Rev Mol Cell Biol* 2023, 24: 560–575
28. Glick D, Barth S, Macleod KF. Autophagy: cellular and molecular mechanisms. *J Pathol* 2010, 221: 3–12
29. Wei X, Tang Z, Wu H, Zuo X, Dong H, Tan L, Wang W, ***et al.*** Biofunctional magnesium-coated Ti6Al4V scaffolds promote autophagy-dependent apoptosis in osteosarcoma by activating the AMPK/mTOR/ULK1 signaling pathway. *Mater Today Bio* 2021, 12: 100147
30. Liu L, Yu Z, Chen J, Liu B, Wu C, Li Y, Xu J, ***et al.*** Lucialdehyde B suppresses proliferation and induces mitochondria-dependent apoptosis in nasopharyngeal carcinoma CNE2 cells. *Pharm Biol* 2023, 61: 918–926
31. Fan M, Chen Z, Shao W, Chen Y, Lin Z, Yi C, Li Y, ***et al.*** SREBP2 inhibitor betulin sensitizes hepatocellular carcinoma to lenvatinib by inhibiting the mTOR/IL-1β pathway. *Acta Biochim Biophys Sin* 2023, 55: 1479–1486
32. Zheng C, Yu X, Liang Y, Zhu Y, He Y, Liao L, Wang D, ***et al.*** Targeting PFKL with penfluridol inhibits glycolysis and suppresses esophageal cancer tumorigenesis in an AMPK/FOXO3a/BIM-dependent manner. *Acta Pharm Sin B* 2022, 12: 1271–1287
33. Yang M, Liu J, Shao J, Qin Y, Ji Q, Zhang X, Du J. Cathepsin S-mediated autophagic flux in tumor-associated macrophages accelerate tumor development by promoting M2 polarization. *Mol Cancer* 2014, 13: 43
34. Zhou C, Zhong W, Zhou J, Sheng F, Fang Z, Wei Y, Chen Y, ***et al.*** Monitoring autophagic flux by an improved tandem fluorescent-tagged LC3 (mTagRFP-mWasabi-LC3) reveals that high-dose rapamycin impairs autophagic flux in cancer cells. *Autophagy* 2012, 8: 1215–1226
35. Ni HM, Bockus A, Wozniak AL, Jones K, Weinman S, Yin XM, Ding WX. Dissecting the dynamic turnover of GFP-LC3 in the autolysosome. *Autophagy* 2011, 7: 188–204
36. Iwai-Kanai E, Yuan H, Huang C, Sayen MR, Perry-Garza CN, Kim L, Gottlieb RA. A method to measure cardiac autophagic flux in vivo. *Autophagy* 2008, 4: 322–329
37. Gong H, Chen H, Xiao P, Huang N, Han X, Zhang J, Yang Y, ***et al.*** miR-146a impedes the anti-aging effect of AMPK via NAMPT suppression and NAD+/SIRT inactivation. *Sig Transduct Target Ther* 2022, 7: 66
38. Hwang JT, Ha J, Park IJ, Lee SK, Baik HW, Kim YM, Park OJ. Apoptotic effect of EGCG in HT-29 colon cancer cells via AMPK signal pathway. *Cancer Lett* 2007, 247: 115–121
39. Vucicevic L, Misirkic M, Kristina J, Vilimanovich U, Sudar E, Isenovic E, Prica M, ***et al.*** Compound C induces protective autophagy in cancer cells through AMPK inhibition-independent blockade of Akt/mTOR pathway. *Autophagy* 2011, 7: 40–50
40. Doki Y, Ajani JA, Kato K, Xu J, Wyrwicz L, Motoyama S, Ogata T, ***et al.*** Nivolumab combination therapy in advanced esophageal squamous-cell carcinoma. *N Engl J Med* 2022, 386: 449–462
41. Lou R, Yang T, Zhang X, Gu J, Xue LJ, Gan D, Li H, ***et al.*** Triptonide induces apoptosis and inhibits the proliferation of ovarian cancer cells by activating the p38/p53 pathway and autophagy. *Bioorg Med Chem* 2024, 110: 117788
42. Ma S, Lu CC, Yang LY, Wang JJ, Wang BS, Cai HQ, Hao JJ, ***et al.*** ANXA2 promotes esophageal cancer progression by activating MYC-HIF1A-VEGF axis. *J Exp Clin Cancer Res* 2018, 37: 183
43. Liu A, Zhu J, Wu G, Cao L, Tan Z, Zhang S, Jiang L, ***et al.*** Antagonizing miR-455-3p inhibits chemoresistance and aggressiveness in esophageal squamous cell carcinoma. *Mol Cancer* 2017, 16: 106
44. Gao B, Chen J, Han B, Zhang X, Hao J, Giuliano AE, Cui Y, ***et al.*** Identification of triptonide as a therapeutic agent for triple negative breast cancer treatment. *Sci Rep* 2021, 11: 2408
45. Strasser A, Vaux DL. Cell death in the origin and treatment of cancer. *Mol Cell* 2020, 78: 1045–1054
46. Hänggi K, Ruffell B. Cell death, therapeutics, and the immune response in cancer. *Trends Cancer* 2023, 9: 381–396
47. Nah J, Zablocki D, Sadoshima J. The role of autophagic cell death in cardiac disease. *J Mol Cell Cardiol* 2022, 173: 16–24
48. Lee MG, Kwon YS, Nam KS, Kim SY, Hwang IH, Kim S, Jang H. Chaga mushroom extract induces autophagy via the AMPK-mTOR signaling pathway in breast cancer cells. *J EthnoPharmacol* 2021, 274: 114081
49. Dong F, Yang P, Wang R, Sun W, Zhang Y, Wang A, Chen M, ***et al.*** Triptonide acts as a novel antiprostate cancer agent mainly through inhibition of mTOR signaling pathway. *Prostate* 2019, 79: 1284–1293
50. Chinison J, Aguilar JS, Avalos A, Huang Y, Wang Z, Cameron DJ, Hao J. Triptonide effectively inhibits Wnt/β-catenin signaling via C-terminal transactivation domain of β-catenin. *Sci Rep* 2016, 6: 32779
51. Wang S, Lv Y, Xu XC, Zuo Y, Song Y, Wu G, Lu PH, ***et al.*** Triptonide inhibits human nasopharyngeal carcinoma cell growth via disrupting LncRNA THOR-IGF2BP1 signaling. *Cancer Lett* 2019, 443: 13–24
52. Zachari M, Ganley Ian G. The mammalian ULK1 complex and autophagy initiation. *Essays Biochem* 2017, 61: 585–596
53. Egan D, Kim J, Shaw RJ, Guan KL. The autophagy initiating kinase ULK1

is regulated via opposing phosphorylation by AMPK and mTOR. *Autophagy* 2011, 7: 643–644
54. Wong PM, Puente C, Ganley IG, Jiang X. The ULK1 complex. *Autophagy* 2013, 9: 124–137
55. Kim YC, Guan KL. mTOR: a pharmacologic target for autophagy regulation. *J Clin Invest* 2015, 125: 25–32
56. Li W, Li D, Ma Q, Chen Y, Hu Z, Bai Y, Xie L. Targeted inhibition of mTOR by BML-275 induces mitochondrial-mediated apoptosis and autophagy in prostate cancer. *Eur J Pharmacol* 2023, 957: 176035
57. Akasaka Y, Hasei S, Ohata Y, Kanna M, Nakatsu Y, Sakoda H, Fujishiro M, *et al.* Auraptene enhances AMP-activated protein kinase phosphorylation and thereby inhibits the proliferation, migration and expression of androgen receptors and Prostate-Specific antigens in prostate cancer cells. *Int J Mol Sci* 2023, 24: 16011
58. Herzig S, Shaw RJ. AMPK: guardian of metabolism and mitochondrial homeostasis. *Nat Rev Mol Cell Biol* 2018, 19: 121–135
59. Fleming A, Bourdenx M, Fujimaki M, Karabiyik C, Krause GJ, Lopez A, Martín-Segura A, *et al.* The different autophagy degradation pathways and neurodegeneration. *Neuron* 2022, 110: 935–966
60. Egan DF, Shackelford DB, Mihaylova MM, Gelino S, Kohnz RA, Mair W, Vasquez DS, *et al.* Phosphorylation of ULK1 (hATG1) by AMP-activated protein kinase connects energy sensing to mitophagy. *Science* 2011, 331: 456–461
61. Kim J, Kundu M, Viollet B, Guan KL. AMPK and mTOR regulate autophagy through direct phosphorylation of Ulk1. *Nat Cell Biol* 2011, 13: 132–141
62. Heng Y, Liang Y, Zhang J, Li L, Zhang W, Jiang Y, Wang S, *et al.* Camptothecin inhibits neddylation to activate the protective autophagy through NF-κB/AMPK/mTOR/ULK1 axis in human esophageal cancer cells. *Front Oncol* 2021, 11: 671180